

Phosphazene functionalized silsesquioxane-based porous polymers for absorbing I₂, CO₂ and dyes

Yiqi Wang^a, Mikhail Soldatov^a, Qingzheng Wang^a, Hongzhi Liu^{a,b,*}

^a Key Laboratory of Special Functional Aggregated Materials, Ministry of Education, School of Chemistry and Chemical Engineering Shandong University, Jinan, PR China

^b Key Laboratory of Organosilicon and Materials Technology of the Ministry of Education, Hangzhou Normal University, Hangzhou, 31112, PR China

ARTICLE INFO

Keywords:
Phosphazene
Silsesquioxane
Adsorption

ABSTRACT

Porous polymers have been widely used as adsorbents to cope with environmental issues. Two parallel series of hybrid silsesquioxane-based phosphazene functionalized porous polymers (PCS-OP-1, 2, 3 and PCS-CP-1, 2, 3) have been prepared by varying the molar ratio of hexaphenoxycyclotriphosphazene (OP) or hexaphenylcyclotriphosphazene (CP) with octavinylsilsesquioxane (OVS) in the Friedel-Crafts reaction, respectively. PCS-OP-3 and PCS-CP-3 with hierarchical micropore/mesopore coexisting structures and high surface areas are chosen to absorb I₂ vapor, dyes and CO₂. The adsorption capacity of PCS-OP-3 is higher than PCS-CP-3, which is 1.51 g g⁻¹ for iodine vapor, 731 mg g⁻¹ for Congo red (CR), 151 mg g⁻¹ for Methylene Blue (MB) and 1.74 mmol g⁻¹ for CO₂. This study provides a feasible method to prepare and tune phosphazene functionalized silsesquioxane-based porous polymers.

1. Introduction

Recently, environmental pollution induced by dyes, CO₂ and radioactive nuclear waste (e.g., ¹²⁹I, ⁸⁵Kr, ¹²⁷Xe) has attracted the attention of governments and organizations worldwide because of its long-term harmful influence on both human health and nature [1–3]. The main sources of pollutants include municipal, industrial and agricultural activities, and it is urgent to find new effective materials and methods for their removal from wastes.

Currently, adsorption is considered as an efficient way to remove pollutants from human activities wastes, due to variability of good adsorbents and its technological simplicity [3–6]. Activated carbon, zeolites and carbon nanotubes were widely used in adsorption with low cost and good reversibility [7–9]. However, the low adsorption capacity and removal efficiency become obstacles to widespread use. Metal-organic frameworks (MOFs) [10–13] is a kind of porous three-dimensional crystal for adsorption due to large specific surface area, while it is water-instable and highly cost. Thus, it is of growing need for finding an ideal adsorbent exhibiting high adsorption capacity, thermal and chemical stability as well as low cost.

Inorganic-organic hybrid porous polymers contain both organic and inorganic units, which make them highly thermally and chemically

stable because of inorganic moieties and easily modified because of organic moieties [14–18]. These above-mentioned properties inspired researchers to study hybrid materials intensely during the recent decades. Cage-like silsesquioxanes (SQs), which have three-dimensional structure, are inorganic-organic hybrid molecules with general chemical formula of (RSiO_{1.5})_n (n = 6, 8, 10–12, 14), where cubic T₈ cages with n = 8 are the most extensively studied [19–25]. SQs possess an excellent chemical and thermal stability, and can react with various substances to prepare micro-mesoporous polymers with high surface area [26–28]. Octavinylsilsesquioxane (OVS) is one of the mostly used cage monomers for preparation of silsesquioxane-based porous materials through hydrosilylation reaction [16,29–31], Heck coupling reaction [28,32], Friedel-Crafts reaction [33–36], cationic polymerization [26] etc. It's worth mentioning that the Friedel-Crafts reaction is a simple method with mild reaction condition, high efficiency and low-cost catalyst to prepare porous polymers in a large scale compared to Heck reaction and hydrosilylation reaction, which need noble catalysts and strict condition [29–33]. Recently, Zhang et al., synthesized a new porous polymer by Friedel-Crafts reaction, which showed an excellent thermal stability and iodine loading capacities (1.37 g g⁻¹ at 90 °C) [37].

The performance of the adsorbents is not only affected by stability,

* Corresponding author. Shandong University, Jinan, PR China.

E-mail address: liuhongzhi@sdu.edu.cn (H. Liu).

<https://doi.org/10.1016/j.polymer.2021.123491>

Received 13 November 2020; Received in revised form 27 January 2021; Accepted 29 January 2021

Available online 4 February 2021

0032-3861/© 2021 Elsevier Ltd. All rights reserved.

but also determined by the typical adsorption parameters, such as the specific surface area and pore volume [33,38]. Moreover, the adsorption performance also depends on functional sites in pores providing strong interaction with the molecules, which ensures the high adsorption capacities [39–43]. Therefore, in order to improve the adsorption capacity of adsorbent for I₂, CO₂ and dyes, we should focus on new strategy to introduce special active sites, or increase porosity as well as stability. For example, we can introduce some rigid or/and heteroatom-containing structures into the adsorbent [37,44,45]. The phosphazene compounds can be easily modified by various functional groups to impart them such unique properties as good biocompatibility, thermal stability and solvent resistance [46], which makes them to be widely applied in biomaterials [47], catalysis [48], flame retardant materials [49], adsorbents [50,51], membranes [52], and so on. For example, Zhang et al. synthesized metal-containing cyclomatrix polyphosphazene materials showing potential applications in charge-selective adsorption [53]. Liu et al. reported organic–inorganic hybrid cyclomatrix polyphosphazene submicron-spheres which can selectively adsorb and separate dyes from an aqueous solution [54]. Soldatov et al. prepared a hybrid phosphazene-containing silsesquioxane-based porous polymer by Heck coupling OVS with hexa (4-bromophenoxy)cyclo-triphosphazene, which showed the highest adsorption capacities for ions such as Pb²⁺, Hg²⁺, Cu²⁺ [32]. Generally, specific binding sites for iodine molecules involve heteroatoms (nitrogen, phosphorus, sulfur and boron) and π bonded fragments (aromatic rings, double and triple bonds) [44]. For example, triphenylamine-functionalized silsesquioxane-based porous polymer prepared by Scholl coupling was employed to capture I₂ vapor and offered a high adsorption capacity of 4 g g⁻¹ within 1 h since it had a high nitrogen atom content and an extended conjugation structure [55]. Thus poly- and cyclophosphazenes, containing alternating phosphorus and nitrogen atoms in the backbone, might serve as efficient iodine adsorbents [56]. Mohanty et al. reported cyclophosphazene based inorganic-organic hybrid nanoporous materials and explored their adsorption of iodine vapor, which resulted in maximum iodine capture capacity of 223 wt% [57]. Geng et al. used biimidazole to react apart with 2,4,6-trichloro-1,3,5-triazine and hexachlorocyclo-triphosphazene by nucleophilic substitution to form POPs (TBIM and HBIM), which showed the astonishing adsorption capacities for iodine molecules with the adsorption capacities of 9.43 and 8.11 g g⁻¹, respectively [58]. However, it has not been reported that combining OVS with cyclophosphazene by Friedel-Crafts reaction to prepare porous materials and using them as adsorbents.

In this work, we selected two typical cyclophosphazene monomers, hexaphenoxycyclo-triphosphazene (OP) and hexaphenylcyclo-triphosphazene (CP), as functional units, and then crosslinked them with octavinylsilsesquioxane (OVS) by Friedel–Crafts reaction catalyzed with AlCl₃. We synthesized two parallel series of phosphazene/silsesquioxane-based functional porous polymers (PCS-OP-1, 2, 3 and PCS-CP-1, 2, 3), which exhibited high specific surface areas and high thermal stabilities. Their porosities can be tuned easily by changing the molar ratio of OP (or CP) with OVS. In this study, we selected PCS-OP-3 and PCS-CP-3 with high surface areas in two parallel series to investigate their applications in adsorbing iodine vapor, dyes and CO₂. The adsorption capacity of PCS-OP-3 is 1.51 g g⁻¹ for iodine vapor, 731 mg g⁻¹ for CR, 151 mg g⁻¹ for MB and 1.74 mmol g⁻¹ for CO₂, which is higher than PCS-CP-3 considering its higher surface area.

2. Experimental

2.1. Materials

Unless otherwise noted, all reagents were purchased from commercial suppliers and used without further purification. Octavinylsilsesquioxane (OVS) was synthesized by previous reports [59]. THF was dried over Na/benzophenone and used as freshly distilled before synthesis. Carbon tetrachloride (CCl₄), triethylamine (Et₃N),

dichloromethane (CH₂Cl₂) and 1,2-dichloroethane (CH₂ClCH₂Cl) were dried over CaH₂ for 12 h and used as freshly distilled.

2.2. Synthesis of monomers (OP and CP)

The monomers OP and CP were prepared according to a similar procedure described in Ref. [60].

Hexaphenoxycyclo-triphosphazene (OP): Sodium phenolate was prepared by adding dropwise phenol (2.0 g, 21.6 mmol) dissolved in 20 mL anhydrous THF to sodium hydride (0.52 g, 21.6 mmol) in the reaction flask. The solution of Hexachlorocyclo-triphosphazene (0.94 g, 2.7 mmol) in 20 mL of dry THF was added slowly via syringe and the mixture was stirred under reflux for 48 h. After reaction, the solution was filtered, washed with brine, dried and the solvent was removed by rotary evaporation. The product was recrystallized from ethyl acetate and dried under vacuum. Yield: (1.6 g, 85%). ¹H NMR (Figure S1(a), 300.53 MHz, CDCl₃, δ): 7.10–7.00 (m, 18H), 6.84 (d, 12 H). ¹³C NMR (Figure S1(b), 75.57 MHz, CDCl₃, δ): 121.09, 124.89, 129.44, 150.64. ³¹P NMR (Figure S1(c), CDCl₃, δ): 8.68 (s).

Hexaphenylcyclo-triphosphazene (CP): Diphenylphosphinamide (2.0 g, 9.2 mmol) and triphenylphosphine (2.9 g, 11.1 mmol) were dissolved in dry dichloromethane (30 mL), carbon tetrachloride (1.3 mL, 9.2 mmol) and triethylamine (1.3 mL, 9.2 mmol), and then the reaction mixture was refluxed at 45 °C for 5 h. After reaction, the mixture was filtered. The solution was washed with brine, dried. After the solvent was removed, the product was recrystallized and dried under vacuum. Yield: (1.4 g, 77%). ¹H NMR (Figure S2(a), 300.53 MHz, CDCl₃, δ): 7.70 (m, 18H), 7.23 (d, 12 H). ¹³C NMR (Figure S2(b), 75.57 MHz, CDCl₃, δ): 127.93, 130.33, 130.76, 139.04. ³¹P NMR (Figure S2(c), CD₂Cl₂, δ): 15.02 (s).

2.3. Synthesis of hybrid porous polymers (PCS-OPs and PCS-CPs)

Typical procedure for PCS-OP-3: The molar ratio of OP to OVS for PCS-OP-3 is 1:3.75. OVS (1.2 g, 1.875 mmol), OP (0.35 g, 0.5 mmol), anhydrous aluminum chloride (1.5 g, 11.3 mmol) and 1,2-dichloroethane (45 mL) were charged in an oven-dried flask. The mixture was first stirred at room temperature for 0.5 h, and then refluxed for 24 h. After cooling to room temperature, the mixture was filtered and solid was washed with THF, methanol, dichloromethane, sequentially, in order to remove unreacted monomers or residual catalyst. The product was further purified under the Soxhlet extractor with methanol for 48 h and dichloromethane for 48 h, respectively, and then dried in vacuum at 80 °C for 24 h to obtain brown solid. Yields: PCS-OP-3 (1.6 g, 103%), PCS-CP-3 (1.8 g, 120%).

Moreover, PCS-OP-1, PCS-OP-2, PCS-CP-1 and PCS-CP-2 were synthesized by OP (or CP) and OVS in different proportions. When the molar ratio of OP (or CP) to OVS was 1: 0.75, PCS-OP-1 and PCS-CP-1 were obtained; when the molar ratio was 1:1.5, PCS-OP-2 and PCS-CP-2 were obtained. Yields: PCS-OP-1 (0.4 g, 68%), PCS-OP-2 (0.8 g, 97%), PCS-CP-1 (0.2 g, 37%), PCS-CP-2 (0.7 g, 90%).

2.4. Procedure for the uptake of I₂ vapor by PCS-OP-3 and PCS-CP-3

A sample of PCS-OP-3 or PCS-CP-3 powder (50.0 mg) and an excess of crystalline iodine were placed in a sealed polypropylene container and heated at 70 °C under ambient pressure. After specific period of time, the container was cooled down to room temperature and the PCS-OP-3 or PCS-CP-3 sample was quickly weighed. The I₂ uptake of PCS-OP-3 or PCS-CP-3 was calculated by weight gain: $\alpha = (m_2 - m_1)/m_1$, where α is the I₂ uptake, m_1 and m_2 are the masses of the PCS-OP-3 or PCS-CP-3 samples before and after being exposed to I₂ vapor, respectively.

2.5. Procedure for the adsorption of dyes by PCS-OP-3 and PCS-CP-3

The solution mode adsorption studies were carried out for aqueous

solution of dyes, including Congo red (CR), and methylene blue (MB). In the process of dyes adsorption, 5 mg of PCS-OP-3 or PCS-CP-3 were dispersed in 20 mL of an aqueous solution of dyes with different concentration. The mixture was stirred at room temperature for 24 h until the equilibrium was reached. The dyes concentration in the solution before and after adsorption was determined by an Ultraviolet-visible (UV-vis) spectrophotometer (497 nm for CR and 664 nm for MB).

2.6. Material characterization

Fourier-transformed infrared (FT-IR) spectra were characterized using a Bruker TENSOR-27 infrared spectrophotometer from 4000 cm^{-1} to 400 cm^{-1} at a resolution of 4 cm^{-1} . The sample was prepared using a conventional KBr disk method. Solid-state ^{13}C CP/MAS NMR, ^{29}Si MAS NMR and ^{31}P MAS NMR spectra were recorded on a Bruker AVANCE-500 NMR spectrometer operating under a magnetic field strength of 9.4 T. The resonance frequencies at this field strength were 125.99 and 202.6 MHz for ^{13}C NMR, ^{29}Si NMR and ^{31}P NMR, respectively. A Chemagnetics 5 mm triple-resonance MAS probe was used to acquire ^{13}C , ^{29}Si and ^{31}P NMR spectra. ^{29}Si NMR spectra with high power proton decoupling were recorded with a $\pi/2$ pulse length of 5 μs , a recycle delay of 120 s, and a spinning rate of 5 kHz. The ^{13}C chemical shifts were referenced externally via the resonance of tetramethylsilane (TMS) of 0 ppm. The ^{31}P chemical shifts were referenced externally via the resonance of $\text{NH}_4\text{H}_2\text{PO}_4$ at an isotropic chemical shift of 1.058 ppm.

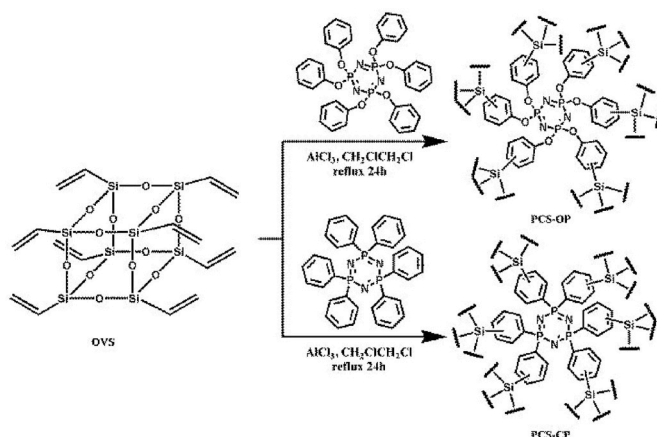
Elemental analysis was conducted using an Elementarvario EL III elemental analyzer. Field-emission scanning electron microscopy (FE-SEM) experiments were characterized using a HITACHI S4800 spectrometer. High-resolution transmission electron microscopy (HR-TEM) experiments were performed using a JEM 2100 electron microscope (JEOL, Japan) with an acceleration voltage of 200 kV. Thermal gravimetric analysis (TGA) was performed on a Mettler-Toledo model SDTA-854 TG A system under a N_2 atmosphere at a heating rate of 10 $^\circ\text{C min}^{-1}$ from room temperature to 800 $^\circ\text{C}$. Powder X-ray diffraction (PXRD) images were collected on a Rigaku D/MAX 2550 diffractometer under $\text{Cu-K}\alpha$ radiation, at 40 kV and 200 mA, with a 2θ range of 5–80 $^\circ$ (scanning rate of 10 $^\circ \text{min}^{-1}$) at room temperature. The UV-vis adsorption spectra of dye solutions were obtained by a TU-1901 spectrophotometer at room temperature.

N_2 sorption isotherm measurements were characterized with a Micromeritics surface area and pore-size analyzer. Before measurement, the samples were degassed for 12 h at 150 $^\circ\text{C}$. A sample of ca. 100 mg and UHP-grade N_2 (99.999%) gas source were adopted in the N_2 sorption measurements at 77 K and collected with a Quantachrome Quadrasorb apparatus. BET surface areas were confirmed over a P/P_0 range from 0.01 to 0.20. Nonlocal density functional theory (NL-DFT) pore-size distributions (PSDs) were determined by using the carbon/slit-cylindrical pore mode of the Quadrawin software. The CO_2 adsorption capacity was measured at 273 K and 1.0 bar. Before measurement, the samples were degassed at 150 $^\circ\text{C}$ under vacuum for about 15 h.

3. Results and discussion

3.1. Synthesis and characterization

The preparation routes for two series of phosphazene/silsesquioxane hybrid porous polymers were depicted in Scheme 1. Hexaphenoxycyclotriphosphazene (OP) and hexaphenylcyclotriphosphazene (CP) were used as phosphazene units and they are different by the presence of oxygen atoms in organic substituents or not. The crosslinking between cyclotriphosphazenes and OVS was performed by Friedel-Crafts reaction with AlCl_3 as catalyst and 1,2-dichloroethane as solvent. Two parallel series of hybrid polymers assigned as PCS-OPs (PCS-OP-1, 2 and 3) and PCS-CPs (PCS-CP-1, 2 and 3) were prepared by varying the molar ratio between OP or CP and OVS, respectively. As two representative samples, PCS-OP-3 with the highest surface area as well as its analogous product



Scheme 1. Preparation of hybrid porous polymers by cross-linking OVS with OP and CP via a Friedel-Crafts reaction, respectively. Some possible fragments formed in the networks are shown as examples.

PCS-CP-3 were used for the further studies.

Infrared spectra of the polymers along with the precursors are shown in Figure S3. The band located at around 1100 cm^{-1} ($\nu_{\text{Si-O-Si}}$) and 1200 cm^{-1} ($\nu_{\text{P=N}}$) segments arises from silsesquioxane and cyclophosphazene units in polymers, respectively. The C-H stretching vibration peak of vinyl groups at 3053 cm^{-1} decreases dramatically after the Friedel-Crafts reaction, and a new peak at 2967 cm^{-1} appears demonstrating the formation of CH_2 linkage, which indicates that the polymers are successfully synthesized. Furthermore, a peak at 3440 cm^{-1} is attributed to Si-OH group, which is formed after Si-O-Si or Si-C bond cleavage caused by AlCl_3 during the reaction.

The solid-state NMR measurements were performed to investigate the structures of PCS-OP-3 and PCS-CP-3. In ^{29}Si spectra signals, the peaks that appeared at approximately -66.5, -69.5 and -79 ppm (Fig. 1) suggested the formation of T_3 units ($\text{T}_n = \text{CSi}(\text{OSi})_n(\text{OH})_{3-n}$), and generation of regioisomers; signals at -100 ppm suggest the formation of Q_3 units ($\text{Q}_n = \text{Si}(\text{OSi})_n(\text{OH})_{4-n}$). Compared with the ^{29}Si MAS NMR spectrum of OVS with one peak at -79 ppm, the presence of Q_n signals is explained by partial collapse of cages in the framework caused by AlCl_3 during Friedel-Crafts reaction. The signal at -80.7 ppm should be assigned to the "Si" atom from unreacted " Si-CH=CH_2 " group, which agreed with the FTIR results, and further revealed there were some unreacted vinyl groups. The relative intensity ratio $\text{T}_3/(\text{T} + \text{Q})$ is up to 0.9 for PCS-OP-3 and 0.8 for PCS-CP-3, which means that less than 20% cages in the network are cleaved.

The solid-state ^{13}C CP/MAS NMR spectra of the PCS-OP-3 and PCS-CP-3 are shown in Figure S4. The broader peaks at about 130 ppm should be assigned to aromatic carbons of OP and CP, as well as the carbon atoms of unreacted vinyl groups [61]. Compared with OVS, the new peaks from 0 to 50 ppm are mainly ascribed to the alkyl carbons of Si- CH_2 - CH_2 -OP (CP) and Si- $\text{CH}(\text{CH}_3)$ OP(CP) units, again confirming that the formation of single C-C bonds derived from vinyl units after Friedel-Crafts reaction. The solid-state ^{31}P MAS NMR spectra of the PCS-OP-3 and PCS-CP-3 are shown in Fig. 2. The spectrum of PCS-OP-3 exhibits a distinct signal at 8.7 ppm (Fig. 2a) and confirms that no reactions happen on phosphazene rings, such as ring opening. The spectrum of PCS-CP-3 exhibits divided signals at 16 and 23 ppm (Fig. 2b) indicating there are reactions on phosphazene rings. The data of solid-state ^{31}P MAS NMR spectra explains the element analysis results (as listed in Table S1) that the content of nitrogen in PCS-CP-3 is lower than PCS-OP-3 and theoretically calculated data.

Therefore, the FT-IR, ^{29}Si NMR, ^{13}C NMR and ^{31}P spectroscopy and element analysis results clearly demonstrate that hexaphenoxycyclotriphosphazene or hexaphenylcyclotriphosphazene can react with OVS by Friedel-Crafts reaction to produce PCS-OP and PCS-CP, respectively.

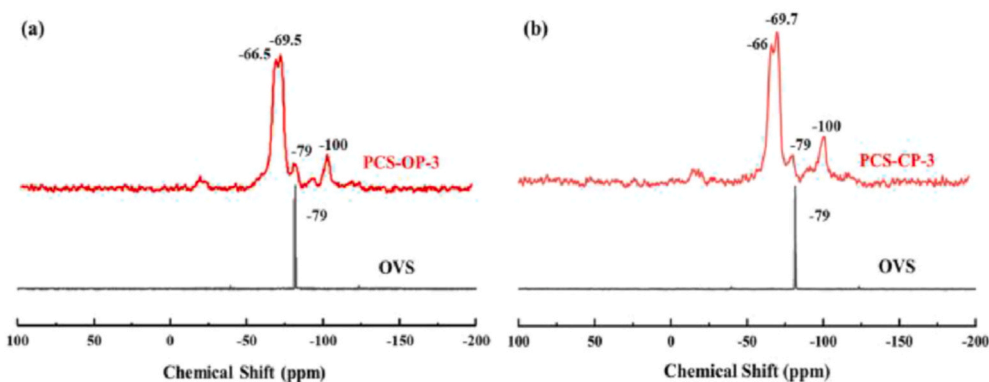


Fig. 1. Solid-state ^{29}Si MAS NMR spectra of OVS, PCS-OP-3 (a) and PCS-CP-3 (b).

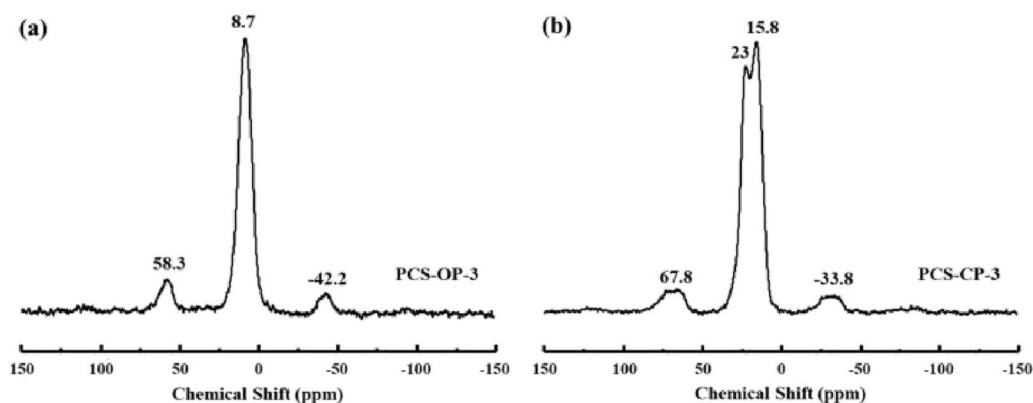


Fig. 2. Solid-state ^{31}P MAS NMR spectra of PCS-OP-3 (a) and PCS-CP-3 (b).

3.2. Thermal property and morphology

It is worth noting that OVS has a good thermal stability ($T_{d5\%} > 280\text{ }^\circ\text{C}$) in air, as shown in Figure S5. The resulted porous polymers showed higher thermal stability than OVS due to the higher crosslinking networks [62]. The 5% weight loss temperature ($T_{d5\%}$) of PCS-CP-3 was $320\text{ }^\circ\text{C}$, which was ca. $30\text{ }^\circ\text{C}$ higher than PCS-OP-3. It can be explained by the presence of P–O bonds in PCS-OP-3, which can decrease thermal stability. Compared with some other OVS-based materials [27,28,38,63], the 5% weight loss temperature ($T_{d5\%}$) of PCSs are lower. This result should be ascribed to the cleavage of partial silsesquioxane cage or ring of phosphazene, which were evidenced from solid state ^{29}Si NMR or ^{31}P NMR spectra. Powder X-ray diffraction (PXRD) analysis was performed to determine the morphology of monomer and resulted materials. As shown in Figure S6, the broad diffraction peaks at about 22° (2θ) demonstrated that although OVS and phosphazene monomers were crystalline, PCS-OP-3 and PCS-CP-3 were amorphous. This may be ascribed to random cross-linking between cages restricting crystalline. In order to analyze the particle size and morphology of PCS-OP-3 and PCS-CP-3, the field emission scanning electron microscopy (FE-SEM) was performed. The FE-SEM images (Figure S7(a), Figure S8(a)) illustrate that samples have irregular shapes and a wide range of diameters from 100 nm to several micrometers. The high-resolution transmission electron microscopy (HR-TEM) images (Figure S7(b), Figure S8(b)) show no evidence to confirm the existence of long-range ordered structures in polymers.

3.3. Porosity

The porosities of the polymers were characterized by N_2 adsorption-desorption measurements at 77 K. As shown in Fig. 3, the fully reversible

isotherms show sharp uptake at low relative pressures, while at higher relative pressure show a gradually increasing tendency in uptake with hysteresis, indicating that the polymers contain both micro- and mesopores. The polymers exhibit the type I and type IV nitrogen sorption isotherms according to the IUPAC classification. Among them, PCS-OP-3 (Fig. 3 (a)) and PCS-CP-3 (Fig. 3 (b)) have H3 hysteresis loop isotherm and there are no obvious saturated adsorption platforms, which indicates that the pore structures are very irregular [64,65].

The Brunauer-Emmett-Teller surface areas (S_{BET}) of PCS-OP-3 and PCS-CP-3 were measured as $686\text{ m}^2\text{ g}^{-1}$ and $462\text{ m}^2\text{ g}^{-1}$ and the micropore surface areas (S_{micro}) were calculated to be $152\text{ m}^2\text{ g}^{-1}$ and $202\text{ m}^2\text{ g}^{-1}$ by the t-plot method, respectively. The presence of oxygen atoms in OP makes the linker between cage and phosphazene ring in PCS-OP-3 more flexible and their relative positions are easily adjusted and optimized. However, some phosphazene rings were cleaved in PCS-CP-3 since the stiff linkage between cage and ring, which can be demonstrated by solid ^{31}P MAS NMR spectra (Fig. 2). Therefore, PCS-OP-3 offers a larger pore volume and higher surface area than PCS-CP-3 [66]. Nonlocal density functional theory (NLDFT) is used to evaluate the pore size distribution (PSD). The PSD curve of PCS-OP-3 showed a unique bimodal structure, which indicated the presence of micropores at $\sim 1.4\text{ nm}$ and mesopores at $\sim 4.2\text{ nm}$, respectively; while the PCS-CP-3 exhibited a hierarchical structure of micropores centered at around 1.7 nm and a relatively broad distribution of mesopores with diameters of $2.9\text{--}10.3\text{ nm}$ due to ring-opening or rearranged phosphazene rings of PCS-CP-3. The total pore volumes (V_{total}) estimated at P/P_0 of 0.99 were separately calculated to be $0.64\text{ cm}^3\text{ g}^{-1}$ and $0.45\text{ cm}^3\text{ g}^{-1}$ for PCS-OP-3 and PCS-CP-3, and the ratios of the micropore volume (V_{micro}) to V_{total} for PCS-OP-3 and PCS-CP-3 were 0.10 and 0.19, respectively. A brief summary of porosity data is listed in Table S2.

PCS-OP-3 and PCS-CP-3 with high surface areas and same molar

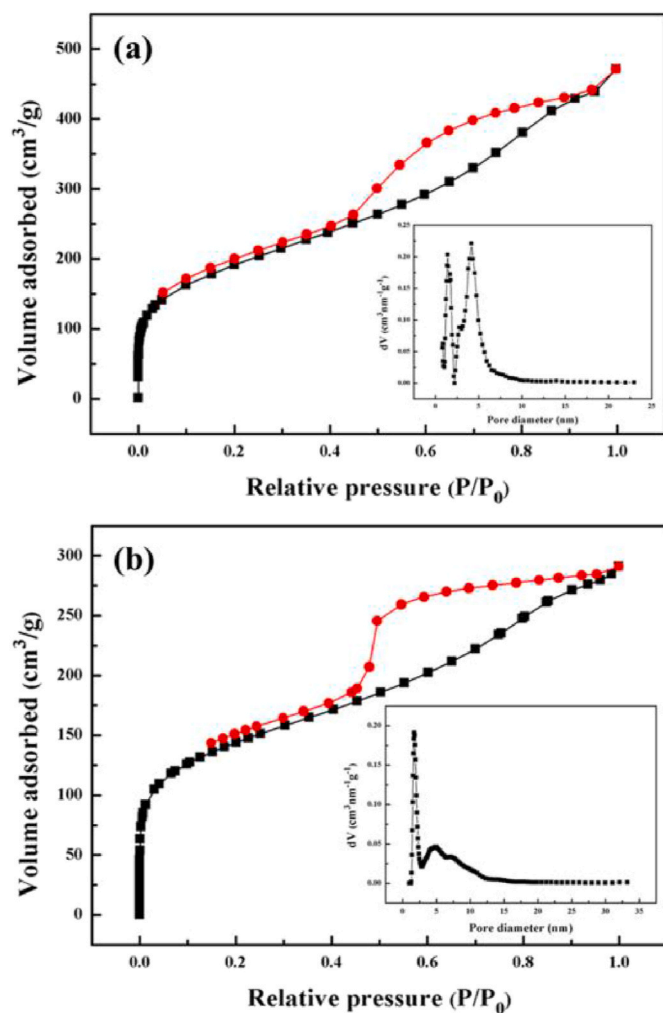


Fig. 3. N₂ adsorption/desorption isotherm and pore size distribution of PCS-OP-3(a) and PCS-CP-3(b).

ratios of reactants in these two parallel series were selected to further investigate their applications in adsorbing iodine vapor, dyes and CO₂, respectively.

3.4. Adsorption of iodine vapor

Since the hybrid porous polymers possess high thermal and chemical stability, high porosity and heteroatoms such as N, P and O in the framework, they were investigated as adsorbents for iodine vapor. Small amounts of the polymers were placed into pre-weighed vials and exposed to I₂ vapor in sealed polypropylene containers. The iodine loading capacities were measured by the weight of samples at different time intervals until no further changes in mass were observed (see the Supporting Information for details). Under ambient pressure and 70 °C, the amount of loaded iodine of PCS-OP-3 and PCS-CP-3 gradually increased at initial 1–2 h, and then reached saturation within 10 h. During the adsorption process, the color of the samples gradually changed from brown to black, which indicated that I₂ had diffused into frameworks of porous polymers (Fig. 4), and the calculated iodine adsorption capacities of PCS-OP-3 and PCS-CP-3 were 1.51 and 1.27 g g⁻¹, respectively.

Previous studies on capture of volatile iodine by porous polymeric adsorbents showed that the adsorption included chemical capture and physical deposition. Among them, the strong affinity of adsorbents to iodine molecules and favorable pore parameters, such as high specific surface area, pore volume and pore size distribution, would lead to

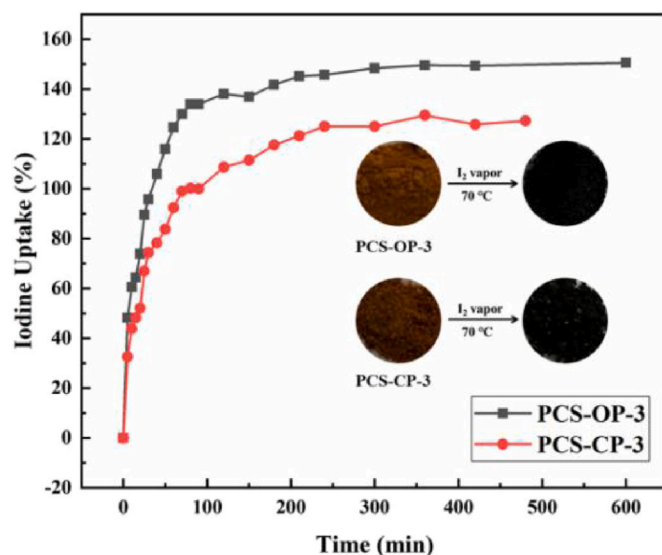


Fig. 4. Iodine uptake curve for PCS-OP-3 and PCS-CP-3 at 70 °C and ambient pressure. Inset: photograph showing the color change of PCS-OP-3 and PCS-CP-3 powder before and after iodine vapor capture. (For interpretation of the references to color in this figure legend, the reader is referred to the Web version of this article.)

increase iodine vapor adsorption capacity [42,44,67,68]. The iodine capture performance may be attributed to three factors: (1) high surface area, considerable pore volume and hierarchical micropore/mesopore provide enough space for iodine capture and good diffusion of iodine molecules into the adsorbent bulk [69,70]; (2) the N-containing frameworks offers binding sites to form N-I halogen bonds and enhance the interaction between iodine molecules and the frameworks [69,71,72]; (3) phosphazene rings with π -conjugations could contribute to efficient iodine uptakes [40,44].

The higher I₂ adsorption capacity in PCS-OP-3 compared to PCS-CP-3 may be ascribed to its higher specific surface area. The diameters of micropores of the polymers are less than 1 nm, close to the dynamic diameters of iodine molecules (0.56 nm), which favor adsorbing iodine vapor molecules [73]. And the mesopore structures of the polymer are helpful for the mass-transfer of iodine molecules, which can improve the adsorption rates of iodine molecules [74]. The adsorption capacities of PCS-OP-3 and PCS-CP-3 for iodine vapor are moderate, perhaps due to the low content of phosphazene rings.

The mechanism of iodine adsorption and the interaction of I₂ with PCS-OP-3 and PCS-CP-3 were studied by FT-IR, TGA, Raman spectroscopy and the energy dispersive X-ray (EDX) spectroscopy. TGA was used to determine the binding strength of adsorbed iodine in the framework. As shown in Figure S9, compared with PCS-OP-3 and PCS-CP-3, the mass loss of PCS-OP-3@I₂ and PCS-CP-3@I₂ was significantly higher. When the temperature reached 281 °C, the weight of PCS-CP-3@I₂ was reduced by 51%. The results are close to the weight increment induced by I₂ capture.

Since N atoms present in the structure, charge transfer in I₂ molecules occurs easily and polarizes into polyiodide (I³⁻, I⁵⁻). The structure of the trapped iodine inside the pores was revealed by Raman spectroscopy (Fig. 5) [70]. The characteristic peaks of PCS-OP-3@I₂ and PCS-CP-3@I₂ were dominated by the peaks around at 107, 142, and 168 cm⁻¹, which were mainly attributed to I³⁻ and I⁵⁻ anions [70]. The strong peak, located at 168 cm⁻¹, attributed to the I⁵⁻ stretching vibration [58]. The characteristic peaks of PCS-OP-3@I₂ at around 107 cm⁻¹, 138 cm⁻¹ and 168 cm⁻¹ belonged to both perturbed di-iodine molecules and asymmetric I³⁻ ions of polyiodides [I³⁻·I₂], whereas the peaks of PCS-CP-3@I₂ at about 142 cm⁻¹ and 168 cm⁻¹ were the results of perturbed di-iodine units for [I⁻(I₂)₂] [68]. The change of

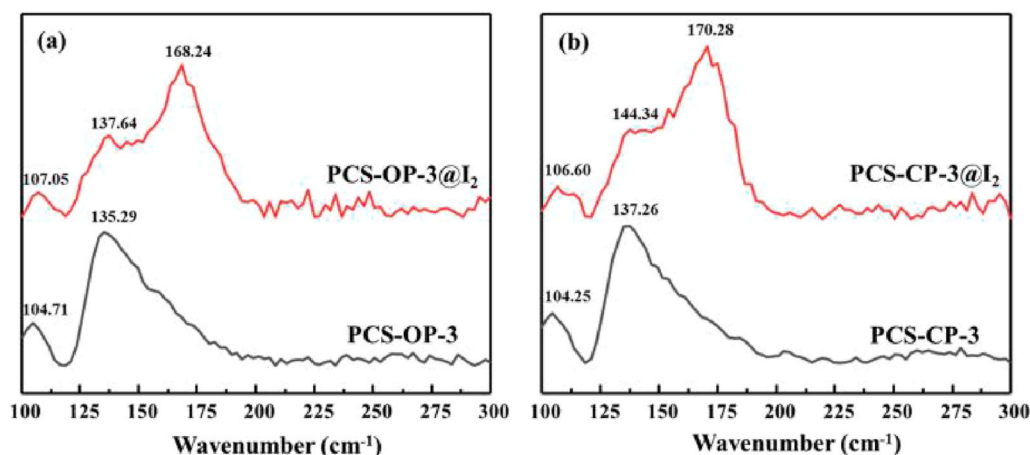


Fig. 5. Raman spectra of PCS-OP-3, PCS-OP-3@I₂(a), PCS-CP-3 and PCS-CP-3@I₂(b).

iodine valence status indicates that chemisorptions occur, which combines with physisorption to obtain a large amount of iodine adsorption [71]. According to the EDX images (Figure S10 and S11), the peaks of P, C and N originated from the framework materials, while the peaks of I arose from the iodine adsorbed on PCS-OP-3@I₂ and PCS-CP-3@I₂, which further revealed that porous polymers could adsorb iodine. The PCS-OP-3@I₂ and PCS-CP-3@I₂ in the air were also compared with those in the iodine atmosphere. It was observed that the mass of polymers in the iodine atmosphere remained same, while the mass of polymers in the air decreased (Figure S12). This means some iodine deposited on the surface of polymers.

Further, the experimental adsorption data of PCS-OP-3 and PCS-CP-3 were simulated with pseudo-first-order and pseudo-second-order kinetic models (Figure S13). As listed in Table S3, the adsorption process matched well with the pseudo-second-order kinetic model which had good linear correlation coefficients R^2 value of more than 0.999. On the basis of the data presented above, the pseudo-second-order kinetic model was more appropriate to describe the adsorption process.

Notably, the trapped iodine can be readily and easily removed from the framework of iodine-loaded materials in organic solvents such as ethanol [55]. For the further study of such releasing process, about 80 mg of PCS-OP-3 or PCS-CP-3 samples and an excess of crystalline iodine were placed in a sealed polypropylene container and heated at 70 °C under ambient pressure for 24 h. After that, the containers were cooled down to room temperature; the PCS-OP-3@I₂ and PCS-CP-3@I₂ sample were quickly weighed. Then, the samples were washed by fresh ethanol, the color of the ethanol solution gradually changed from colorless to orange, which clearly indicated that the iodine molecules were desorbed from the polymeric frameworks. Then the samples were dried under vacuum at 60 °C for 24 h, the quantities of PCS-OP-3 and PCS-CP-3 had not obviously changed by weighing. The regenerated PCS-OP-3 and PCS-CP-3 samples were reused for next cycle by exposing to iodine vapor again. As shown in Fig. 6, after five adsorption cycles, the adsorption abilities of PCS-OP-3 and PCS-CP-3 showed a decrease, because the polymers had N binding sites and the charge transfer in the I₂ molecule can easily occur in the I₂ molecules and polarize into polyiodide, which is not easy to wash off, but the removal capacities were stable above 60% [72]. The two polymers of PCS-OP-3 and PCS-CP-3 after five cycles were denoted as PCS-OP-3-I₂ and PCS-CP-3-I₂, respectively. The FTIR and BET analyses were used to characterize the stabilities of PCS-OP-3-I₂ and PCS-CP-3-I₂. The FTIR spectra shown in Figure S14 indicate that there are no significant differences in the structures of samples before and after 5 cycles of iodine vapor adsorption. Compared with PCS-OP-3 and PCS-CP-3, S_{BET} of PCS-OP-3-I₂ and PCS-CP-3-I₂ decreased to 396.7 and 95.2 m² g⁻¹, respectively (Figure S15 and Table S4). It is explained that some pores are blocked by residual iodine [75]. The cyclic experiments

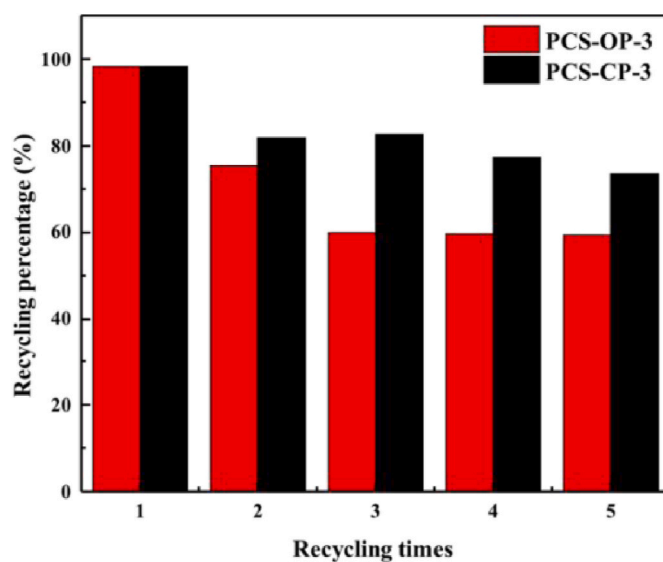


Fig. 6. Recyclability of PCS-OP-3 and PCS-CP-3 for capturing iodine from vapor.

reveal that the polymers could be attractive recyclable adsorbents for iodine vapor capture in practical application.

3.5. Dyes adsorption

It is noteworthy that porous materials were capable for removing dyes from aqueous solution, so the dyes adsorption of PCS-OP-3 and PCS-CP-3 was further studied. In order to estimate the adsorption behavior of PCS-OP-3 and PCS-CP-3 in dye-water solution, an UV-vis spectrophotometer was employed to measure the changes in intensities of the maximum absorption wavelengths of model dyes, Congo red (CR) and Methylene Blue (MB).

As shown in Fig. 7, the initial adsorption amount was a function of the initial concentration of dye solutions, while the adsorption capacities reached the maximum value having nothing to do with the increasing dyes concentrations. The experimental results indicated that the maximum equilibrium adsorption capacity (Q_e) of the two adsorbents in water were 731 and 151 mg g⁻¹ for CR and MB onto PCS-OP-3, respectively, and 522 and 73 mg g⁻¹ for CR and MB onto PCS-CP-3. The Q_e of PCS-OP-3 was larger than that of PCS-CP-3, regardless of dyes, which was due its higher S_{BET} and V_{total} . In addition, the PCS-OP-3 possesses more electron-rich oxygen atoms than PCS-CP-3, which

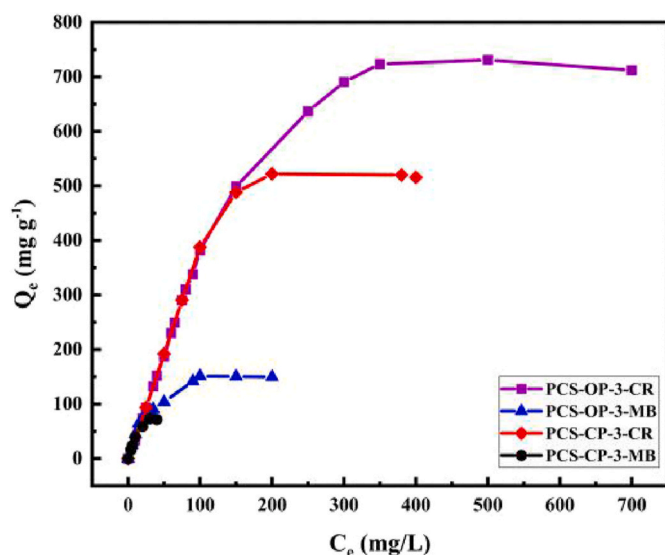


Fig. 7. Equilibrium adsorption isotherms of dyes on PCS-OP-3 and PCS-CP-3.

easily bind cationic dyes through the coulombic force [33,38]. As listed in Table S5, MB is a small-sized cationic dye, while CR is opposite. For PCS-OP-3 and PCS-CP-3, the adsorption capacity of CR was higher than that of MB, indicating that larger dyes could enter the mesopores and be blocked by micropores, whereas small-sized dyes could easily enter and leave the pores [27,45].

In order to further study the adsorption behavior from a theoretical perspective, the isotherm curves were analyzed according to Langmuir and Freundlich models. The related parameters are listed in Table S6 and the details are shown in Figure S16. The correlation coefficients of Langmuir isotherm model showed a better linear fitting than the correlation coefficients of Freundlich isotherm model, indicating that monolayer adsorption occurred in a finite number of identical sites for PCS-OP-3 and PCS-CP-3.

In order to obtain the equilibrium time and fully understand the adsorption mechanism, the adsorption kinetics of PCS-OP-3 and PCS-CP-3 in CR aqueous solution were studied. As shown in Figure S17, we can see that the kinetic adsorption curves can be divided into two stages: the dye adsorption efficiency increased rapidly during the first 40 min, and then a slow increase was observed until it reached equilibrium. The removal efficiencies of 94% and 95% were individually calculated by adsorption data for CR solutions of PCS-OP-3 and PCS-CP-3 at 3 h, respectively.

Pseudo-first-order and pseudo-second-order kinetic models were used to study the adsorption mechanism and the correlative kinetic parameter and curves are listed in Table S7 and Figure S18. In comparison with the pseudo-first-order model, the pseudo-second-order model shows a better linear fitting with the correlation coefficient (R^2) values of 0.9989 and 0.9995 for PCS-OP-3 and PCS-CP-3, respectively.

The encapsulated dyes can be easily removed from the framework of dye-loaded materials in organic solvents. To further study of this releasing process, PCS-OP-3 and PCS-CP-3 were dispersed in the solution of CR with concentration of 40 mg L^{-1} for 24 h, and the residual CR concentration was measured by UV-Vis spectroscopy. After that, the dye-loaded samples were soaked sequentially into fresh methanol and 2 M hydrochloric acid, the color of the methanol solution gradually changed from colorless to orange, which clearly indicated that CR molecules were desorbed from the polymer frameworks. As shown in Fig. 8, after five cycles, the adsorption capacities of PCS-OP-3 and PCS-CP-3 still remain same, revealing that the porous polymers could be promising and recyclable adsorbents for removal of dyes from wastewater.

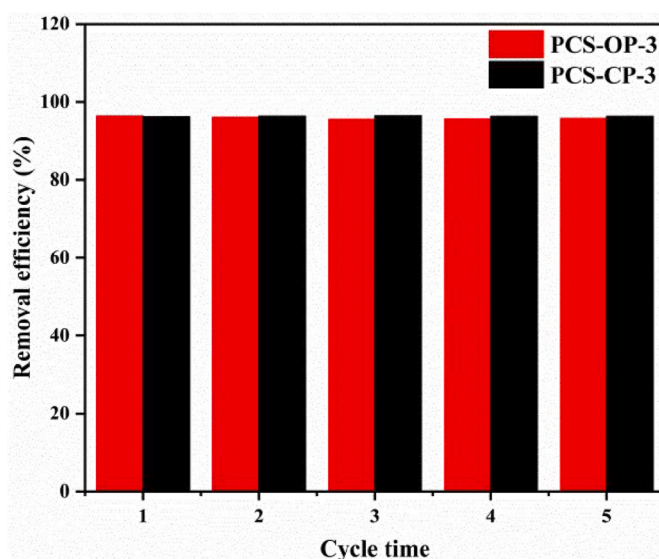


Fig. 8. Recyclability of PCS-OP-3 and PCS-CP-3 for capturing CR.

3.6. CO₂ capture

The mitigation of carbon dioxide emission into the atmosphere has attracted tremendous attention due to the fact that the excessive emission of CO₂ into the atmosphere may cause “greenhouse effect” [76]. Among the different strategies for CO₂ abatement, capture and storage are considered to be advantageous owing to the low energy consumption and ease of operation [77,78]. Therefore, it is vital to develop practical and effective materials with high CO₂ adsorption capacity. Porous materials based on cage-like organosiloxanes (PCSs) have been attempted to store CO₂ by virtue of their abundant porosities [79,80]. The CO₂ adsorption curves of PCS-OP-3 and PCS-CP-3 are shown in Fig. 9. The adsorption capacities of PCS-OP-3 and PCS-CP-3 are calculated as 1.74 mmol g^{-1} (7.65 wt%) and 1.31 mmol g^{-1} (5.76 wt%) at 273.0 K/101 kPa, respectively, which are higher or comparable in comparison with some other PCSs [27,38,63,81]. The higher surface area of PCS-OP-3 accounted for its larger CO₂ adsorption capacity compared to PCS-CP-3.

The high CO₂ adsorption capacities of PCS-OP-3 and PCS-CP-3 can be associated with basic nitrogen atoms in the network, which increase the affinity of the polymers to carbon dioxide molecules via dipole-quadrupole interaction between CO₂ and nitrogen, thereby enhancing the CO₂ adsorption performance [55]. In addition, the porous polymers

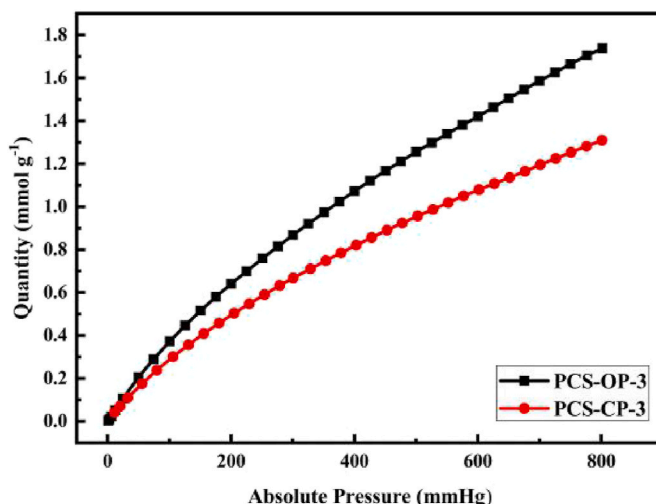


Fig. 9. CO₂ adsorption isotherms of PCS-OP-3 and PCS-CP-3 at 273 K.

possess high specific surface areas and π - π interaction between polymers and carbon dioxide, which also play significant roles in CO₂ adsorption [55,82].

4. Conclusion

In summary, we synthesized two parallel series of silsesquioxane-based phosphazene functionalized porous polymers of PCS-OPs and PCS-CPs via Friedel-Crafts reaction. The high surface area, considerable pore volume, hierarchical micropore/mesopore and N, P-containing frameworks of the polymers enhance the interaction with pollutants, which are conducive to improving adsorption capacities. They exhibited good adsorption abilities for iodine vapor, dyes and CO₂, and PCS-OP-3 showed higher adsorption capacities for iodine vapor, CR and CO₂ with 1.51, 0.73 g g⁻¹ and 1.74 mmol g⁻¹, respectively. Moreover, PCS-OP-3 and PCS-CP-3 showed a good recyclability and can be reused at least for five cycles. All these results show the perspectives of phosphazene containing PCSs for adsorbing iodine vapor, dyes and CO₂.

Declaration of competing interest

The authors declare that they have no known competing financial interests or personal relationships that could have appeared to influence the work reported in this paper.

Acknowledgements

This research was supported by the National Natural Science Foundation of China (NSFC) (No. 21975144), Key Research and Development Program of Shandong province (No. 2019GHZ034), Ministry of Science and Technology of the People's Republic of China and Seed Fund Program for the International Research Cooperation of Shandong University.

Appendix A. Supplementary data

Supplementary data to this article can be found online at <https://doi.org/10.1016/j.polymer.2021.123491>.

References

- [1] H. Sadegh, G.A.M. Ali, V.K. Gupta, A.S.H. Makhlof, R. Shahryari ghoshekandi, M. N. Nadagouda, M. Sillanpää, E. Megiel, The role of nanomaterials as effective adsorbents and their applications in wastewater treatment, *J. Nanostruct. Chem.* 7 (1) (2017) 1–14.
- [2] X. Wang, L. Chen, L. Wang, Q. Fan, D. Pan, J. Li, F. Chi, Y. Xie, S. Yu, C. Xiao, F. Luo, J. Wang, X. Wang, C. Chen, W. Wu, W. Shi, S. Wang, X. Wang, Synthesis of novel nanomaterials and their application in efficient removal of radionuclides, *Sci. China Chem.* 62 (8) (2019) 933–967.
- [3] S.U. Nandanwar, K. Coldsnow, V. Utgikar, P. Sabharwall, D. Eric Aston, Capture of harmful radioactive contaminants from off-gas stream using porous solid sorbents for clean environment – a review, *Chem. Eng. J.* 306 (2016) 369–381.
- [4] J. Huve, A. Ryzhikov, H. Nouali, V. Lalia, G. Augé, T.J. Daou, Porous sorbents for the capture of radioactive iodine compounds: a review, *RSC Adv.* 8 (51) (2018) 29248–29273.
- [5] H. Gao, R. Cao, S. Zhang, H. Yang, X. Xu, Three-dimensional hierarchical g-C₃N₄ architectures assembled by ultrathin self-doped nanosheets: extremely facile hexamethylenetetramine activation and superior photocatalytic hydrogen evolution, *ACS Appl. Mater. Interfaces* 11 (2) (2019) 2050–2059.
- [6] H. Yang, R. Cao, P. Sun, J. Yin, S. Zhang, X. Xu, Constructing electrostatic self-assembled 2D/2D ultra-thin ZnIn₂S₄/protonated g-C₃N₄ heterojunctions for excellent photocatalytic performance under visible light, *Appl. Catal., B* 256 (2019) 117862.
- [7] S.T. Akar, R. Uysal, Untreated clay with high adsorption capacity for effective removal of C.I. Acid Red 88 from aqueous solutions: batch and dynamic flow mode studies, *Chem. Eng. J.* 162 (2) (2010) 591–598.
- [8] E. Kacan, Optimum BET surface areas for activated carbon produced from textile sewage sludges and its application as dye removal, *J. Environ. Manag.* 166 (2016) 116–123.
- [9] H.P.C. van Kuringen, G.M. Eikelboom, I.K. Shishmanova, D.J. Broer, A.P.H. J. Schenning, Responsive nanoporous smectic liquid crystal polymer networks as efficient and selective adsorbents, *Adv. Funct. Mater.* 24 (32) (2014) 5045–5051.
- [10] W. Xie, D. Cui, S.-R. Zhang, Y.-H. Xu, D.-L. Jiang, Iodine capture in porous organic polymers and metal-organic frameworks materials, *Mater. Horiz.* 6 (8) (2019) 1571–1595.
- [11] B. Lee, D. Moon, J. Park, Microscopic and mesoscopic dual postsynthetic modifications of metal-organic frameworks, *Angew. Chem., Int. Ed. Engl.* 132 (33) (2020) 13897–13903.
- [12] G. Brunet, D.A. Safin, M.Z. Aghaji, K. Robeyns, I. Korobkov, T.K. Woo, M. Murugesu, Stepwise crystallographic visualization of dynamic guest binding in a nanoporous framework, *Chem. Sci.* 8 (4) (2017) 3171–3177.
- [13] F. Ahmadijokani, R. Mohammadkhani, S. Ahmadiyouya, A. Shokrgozar, M. Rezakazemi, H. Molavi, T.M. Aminabhavi, M. Arjmand, Superior chemical stability of UiO-66 metal-organic frameworks (MOFs) for selective dye adsorption, *Chem. Eng. J.* 399 (2020) 125346.
- [14] C.F. Lee, D.A. Leigh, R.G. Pritchard, D. Schultz, S.J. Teat, G.A. Timco, R. E. Winpenny, Hybrid organic-inorganic rotaxanes and molecular shuttles, *Nature* 458 (7236) (2009) 314–318.
- [15] S. Seo, W. Chaikittisilp, N. Koike, T. Yokoi, T. Okubo, Porous inorganic-organic hybrid polymers derived from cyclic siloxane building blocks: effects of substituting groups on mesoporous structures, *Microporous Mesoporous Mater.* 278 (2019) 212–218.
- [16] L. Zhang, H.C. Abbenhuis, Q. Yang, Y.M. Wang, P.C. Magusin, B. Mezari, R.A. van Santen, C. Li, Mesoporous organic-inorganic hybrid materials built using polyhedral oligomeric silsesquioxane blocks, *Angew. Chem., Int. Ed. Engl.* 46 (26) (2007) 5003–5006.
- [17] C. Sanchez, G.J.d.A.A. Soler-Illia, F. Ribot, T. Lalot, C.R. Mayer, V. Cabuil, Designed hybrid organic-inorganic nanocomposites from functional nanobuilding blocks, *Chem. Mater.* 13 (2001) 3061–3083.
- [18] J.D. Lichtenhan, K. Pielichowski, I. Blanco, POSS-based polymers, *Polymers* 11 (1727) (2019).
- [19] A. Sellinger, R.M. Laine, Silsesquioxanes as synthetic platforms. Thermally curable and photocurable inorganic/organic hybrids, *Macromolecules* 29 (1996) 2327–2330.
- [20] Y. Itami, B. Marciniak, M. Kubicki, Functionalization of octavinylsilsesquioxane by ruthenium-catalyzed silylative coupling versus cross-metathesis, *Chem. Eur. J.* 10 (5) (2004) 1239–1248.
- [21] M.Z. Asuncion, R.M. Laine, Fluoride rearrangement reactions of polyphenyl- and polyvinylsilsesquioxanes as a facile route to mixed functional phenyl, vinyl T₁₀ and T₁₂ silsesquioxanes, *J. Am. Chem. Soc.* 132 (2010), 3723–3731.
- [22] C. Zhang, R.M. Laine, Hydrosilylation of allyl alcohol with [HSiMe₂OSiO_{1.5}]₈: octa (3-hydroxypropyldimethylsilyloxy)octasilsesquioxane and its octamethacrylate derivative as potential precursors to hybrid nanocomposites, *J. Am. Chem. Soc.* 122 (2000) 6979–6988.
- [23] D.B. Cordes, P.D. Lickiss, F. Rataboul, Recent developments in the chemistry of cubic polyhedral oligosilsesquioxanes, *Chem. Rev.* 110 (2010) 2081–2173.
- [24] M.G. Mohamed, S.W. Kuo, Functional silica and carbon nanocomposites based on polybenzoxazines, *Macromol. Chem. Phys.* 220 (1) (2019) 1800306.
- [25] M.G. Mohamed, S.W. Kuo, Functional polyimide/polyhedral oligomeric silsesquioxane nanocomposites, *Polymers* 11 (26) (2018).
- [26] Y. Du, M. Ge, H. Liu, Porous polymers derived from octavinylsilsesquioxane by cationic polymerization, *Macromol. Chem. Phys.* 220 (5) (2019) 1800536.
- [27] H. Liu, H. Liu, Selective dye adsorption and metal ion detection using multifunctional silsesquioxane-based tetraphenylethene-linked nanoporous polymers, *J. Mater. Chem.* 5 (19) (2017) 9156–9162.
- [28] M. Ge, H. Liu, A silsesquioxane-based thiophene-bridged hybrid nanoporous network as a highly efficient adsorbent for wastewater treatment, *J. Mater. Chem.* 4 (42) (2016) 16714–16722.
- [29] J.J. Morrison, C.J. Love, B.W. Manson, I.J. Shannon, R.E. Morris, Synthesis of functionalised porous network silsesquioxane polymers, *J. Mater. Chem.* 12 (11) (2002) 3208–3212.
- [30] P.A. Agaskar, Organolithitic macromolecular materials derived from vinyl-functionalized spherulites: novel potentially microporous solids, *J. Am. Chem. Soc.* 111 (1989) 6858–6859.
- [31] C. Ling, F. Babonneau, C. Bonhomme, R.M. Laine, C.L. Soles, H.A. Hristov, A. F. Yee, Highly porous polyhedral silsesquioxane polymers. Synthesis and characterization, *J. Am. Chem. Soc.* 120 (1998) 8380–8391.
- [32] M. Soldatov, H. Liu, A POSS-phosphazene based porous material for adsorption of metal ions from water, *Chem. Asian J.* 14 (23) (2019) 4345–4351.
- [33] X. Yang, H. Liu, Diphenylphosphine-substituted ferrocene/silsesquioxane-based hybrid porous polymers as highly efficient adsorbents for water treatment, *ACS Appl. Mater. Interfaces* 11 (29) (2019) 26474–26482.
- [34] X. Yang, G. Yin, Z. Li, P. Wu, X. Jin, Q. Li, The preparation and chemical structure analysis of novel POSS-based porous materials, *Materials* 12 (12) (2019).
- [35] R. Dawson, L.A. Stevens, T.C. Drage, C.E. Snape, M.W. Smith, D.J. Adams, A. I. Cooper, Impact of water coadsorption for carbon dioxide capture in microporous polymer sorbents, *J. Am. Chem. Soc.* 134 (26) (2012) 10741–10744.
- [36] J. Liu, Y. Liu, X. Jiang, Y. Luo, Y. Lyu, POSS-based microporous polymers: efficient Friedel-Crafts synthesis, CO₂ capture and separation properties, *Microporous Mesoporous Mater.* 250 (2017) 203–209.
- [37] W. Zhang, Y. Mu, X. He, P. Chen, S. Zhao, C. Huang, Y. Wang, J. Chen, Robust porous polymers bearing phosphine oxide/chalcogenide ligands for volatile iodine capture, *Chem. Eng. J.* 379 (2020) 122365.
- [38] X. Yang, H. Liu, Ferrocene-functionalized silsesquioxane-based porous polymer for efficient removal of dyes and heavy metal ions, *Chem. Eur. J.* 24 (51) (2018) 13504–13511.

- [39] G. Li, Y. Huang, J. Lin, C. Yu, Z. Liu, Y. Fang, Y. Xue, C. Tang, Effective capture and reversible storage of iodine using foam-like adsorbents consisting of porous boron nitride microfibrils, *Chem. Eng. J.* 382 (2020) 122833.
- [40] Y. Yang, X. Xiong, Y. Fan, Z. Lai, Z. Xu, F. Luo, Insight into volatile iodine uptake properties of covalent organic frameworks with different conjugated structures, *J. Solid State Chem.* 279 (2019) 120979.
- [41] X. Zhang, I. da Silva, H.G.W. Godfrey, S.K. Callear, S.A. Sapchenko, Y. Cheng, I. Vitorica-Yrezabal, M.D. Frogley, G. Cinque, C.C. Tang, C. Giacobbe, C. Dejoie, S. Rudic, A.J. Ramirez-Cuesta, M.A. Denecke, S. Yang, M. Schroder, Confinement of iodine molecules into triple-helical chains within robust metal-organic frameworks, *J. Am. Chem. Soc.* 139 (45) (2017) 16289–16296.
- [42] X. Qian, Z.Q. Zhu, H.X. Sun, F. Ren, P. Mu, W. Liang, L. Chen, A. Li, Capture and reversible storage of volatile iodine by novel conjugated microporous polymers containing thiophene units, *ACS Appl. Mater. Interfaces* 8 (32) (2016) 21063–21069.
- [43] M. Naushad, A.A. Alqadami, Z.A. AlOthman, I.H. Alsohaimi, M.S. Algamdi, A. M. Aldawsari, Adsorption kinetics, isotherm and reusability studies for the removal of cationic dye from aqueous medium using arginine modified activated carbon, *J. Mol. Liq.* 293 (2019) 111442.
- [44] S. Xiong, J. Tao, Y. Wang, J. Tang, C. Liu, Q. Liu, Y. Wang, G. Yu, C. Pan, Uniform poly(phosphazene-triazine) porous microspheres for highly efficient iodine removal, *Chem. Commun.* 54 (61) (2018) 8450–8453.
- [45] C. Zhang, P.-C. Zhu, L. Tan, J.-M. Liu, B. Tan, X.-L. Yang, H.-B. Xu, Triptycene-based hyper-cross-linked polymer sponge for gas storage and water treatment, *Macromolecules* 48 (23) (2015) 8509–8514.
- [46] L. Zhu, Y. Xu, W. Yuan, J. Xi, X. Huang, X. Tang, S. Zheng, One-pot synthesis of poly(cyclotriphosphazene-co-4,4'-sulfonyldiphenol) nanotubes via an In Situ template Approach, *Adv. Mater.* 18 (22) (2006) 2997–3000.
- [47] Y.E. Greish, J.D. Bender, S. Lakshmi, P.W. Brown, H.R. Allcock, C.T. Laurencin, Low temperature formation of hydroxyapatite-poly(alkyl oxybenzoate) phosphazene composites for biomedical applications, *Biomaterials* 26 (1) (2005) 1–9.
- [48] M. Wang, J. Fu, D. Huang, C. Zhang, Q. Xu, Silver nanoparticles-decorated polyphosphazene nanotubes: synthesis and applications, *Nanoscale* 5 (17) (2013) 7913–7919.
- [49] T. Zhang, Q. Cai, D.-Z. Wu, R.-G. Jin, Phosphazene cyclomatrix network polymers: some aspects of the synthesis, characterization, and flame-retardant mechanisms of polymer, *J. Appl. Polym. Sci.* 95 (4) (2005) 880–889.
- [50] C. Chen, X.-y. Zhu, Q.-l. Gao, F. Fang, L.-w. Wang, X.-j. Huang, Immobilization of lipase onto functional cyclomatrix polyphosphazene microspheres, *J. Mol. Catal. B Enzym.* 132 (2016) 67–74.
- [51] Z. Ma, Y. Wang, M. Liu, Y. Luo, X. Xie, Z. Xiong, Highly efficient uranium(VI) removal from aqueous solution using poly(cyclotriphosphazene-co-4,4'-diaminodiphenyl-ether) crosslinked microspheres, *J. Radioanal. Nucl. Chem.* 321 (3) (2019) 1093–1107.
- [52] C.J. Orme, F.F. Stewart, Mixed gas hydrogen sulfide permeability and separation using supported polyphosphazene membranes, *J. Membr. Sci.* 253 (1–2) (2005) 243–249.
- [53] J. Zhang, Z. Miao, J. Yan, X. Zhang, X. Li, Q. Zhang, Y. Yan, Synthesis of negative-charged metal-containing cyclomatrix polyphosphazene microspheres based on polyoxometalates and application in charge-selective dye adsorption, *Macromol. Rapid Commun.* 40 (17) (2019) 1800730.
- [54] W. Wei, R. Lu, H. Xie, Y. Zhang, X. Bai, L. Gu, R. Da, X. Liu, Selective adsorption and separation of dyes from an aqueous solution on organic-inorganic hybrid cyclomatrix polyphosphazene submicro-spheres, *J. Mater. Chem.* 3 (8) (2015) 4314–4322.
- [55] Q. Wang, H. Liu, C. Jiang, H. Liu, Silsesquioxane-based triphenylamine functionalized porous polymer for CO₂, I₂ capture and nitro-aromatics detection, *Polymer* 186 (2020) 122004.
- [56] Y. Dong, S. Chen, X. Lu, Q. Lu, High-level extraction of recyclable nanocatalysts by using polyphosphazene microparticles, *Langmuir* 35 (15) (2019) 5168–5175.
- [57] R. Muhammad, P. Mohanty, Iodine sequestration using cyclophosphazene based inorganic-organic hybrid nanoporous materials: role of surface functionality and pore size distribution, *J. Mol. Liq.* 283 (2019) 58–64.
- [58] T. Geng, C. Zhang, M. Liu, C. Hu, G. Chen, Preparation of biimidazole-based porous organic polymers for ultrahigh iodine capture and formation of liquid complexes with iodide/polyiodide ions, *J. Mater. Chem.* 8 (5) (2020) 2820–2826.
- [59] D. Chen, S. Yi, W. Wu, Y. Zhong, J. Liao, C. Huang, W. Shi, Synthesis and characterization of novel room temperature vulcanized (RTV) silicone rubbers using Vinyl-POSS derivatives as cross linking agents, *Polymer* 51 (17) (2010) 3867–3878.
- [60] P. Schrogel, M. Hoping, W. Kowalsky, A. Hunze, G. Wagenblast, C. Lennartz, P. Strohriegel, Phosphazene-based host materials for the use in blue phosphorescent organic light-emitting diodes, *Chem. Mater.* 23 (2011) 4947–4953.
- [61] M. Ge, H. Liu, Fluorine-containing silsesquioxane-based hybrid porous polymers mediated by bases and their use in water remediation, *Chem. Eur J.* 24 (9) (2018) 2224–2231.
- [62] M.F. Roll, J.W. Kampf, R.M. Laine, Halogen bonding motifs in polyhedral phenylsilsesquioxanes: effects of systematic variations in geometry or substitution, *Cryst. Growth Des.* 11 (10) (2011) 4360–4367.
- [63] Y. Du, H. Liu, Silsesquioxane-based hexaphenylsilo-linked hybrid porous polymer as an effective fluorescent chemosensor for metal ions, *Chemistry* 3 (6) (2018) 1667–1673.
- [64] Q. Chen, M. Luo, P. Hammershøj, D. Zhou, Y. Han, B.W. Laursen, C.G. Yan, B. H. Han, Microporous polycarbazole with high specific surface area for gas storage and separation, *J. Am. Chem. Soc.* 134 (14) (2012) 6084–6087.
- [65] K.W. Sing, Reporting physisorption data for gas/solid systems with special reference to the determination of surface area and porosity (Recommendations 1984), *Pure Appl. Chem.* 57 (4) (1985) 603–619.
- [66] J.X. Jiang, F. Su, A. Trewin, C.D. Wood, N.L. Campbell, H. Niu, C. Dickinson, A. Y. Ganin, M.J. Rosseinsky, Y.Z. Khimyak, A.I. Cooper, Conjugated microporous poly(aryleneethynylene) networks, *Angew. Chem., Int. Ed. Engl.* 46 (45) (2007) 8574–8578.
- [67] Q.M. Zhang, T.L. Zhai, Z. Wang, G. Cheng, H. Ma, Q.P. Zhang, Y.H. Zhao, B. Tan, C. Zhang, Hyperporous carbon from triptycene-based hypercrosslinked polymer for iodine capture, *Adv. Mater. Interfaces* 6 (9) (2019) 1900249.
- [68] C. Pei, T. Ben, S. Xu, S. Qiu, Ultrahigh iodine adsorption in porous organic frameworks, *J. Mater. Chem.* 2 (20) (2014) 7179–7187.
- [69] Y.-Y. Ren, W. Zhang, Y. Zhu, D.-G. Wang, G. Yu, G.-C. Kuang, Nitrogen-rich porous polyaminal network as a platform for iodine adsorption through physical and chemical interaction, *J. Appl. Polym. Sci.* 135 (15) (2018) 46106.
- [70] Y. Wang, J. Tao, S. Xiong, P. Lu, J. Tang, J. He, M.U. Javaid, C. Pan, G. Yu, Ferrocene-based porous organic polymers for high-affinity iodine capture, *Chem. Eng. J.* 380 (2020) 122420.
- [71] H. Li, X. Ding, B.H. Han, Porous azo-bridged porphyrin-phthalocyanine network with high iodine capture capability, *Chem. Eur J.* 22 (33) (2016) 11863–11868.
- [72] D. An, L. Li, Z. Zhang, A.M. Asiri, K.A. Alamry, X. Zhang, Amino-bridged covalent organic Polycalix[4]arenes for ultra efficient adsorption of iodine in water, *Mater. Chem. Phys.* 239 (2020) 122328.
- [73] Z. Guo, P. Sun, X. Zhang, J. Lin, T. Shi, S. Liu, A. Sun, Z. Li, Amorphous porous organic polymers based on schiff-base chemistry for highly efficient iodine capture, *Chem. Asian J.* 13 (16) (2018) 2046–2053.
- [74] P. Wang, Q. Xu, Z. Li, W. Jiang, Q. Jiang, D. Jiang, Exceptional iodine capture in 2D covalent organic frameworks, *Adv. Mater.* (2018) 1801991.
- [75] Y. Du, M. Unno, H. Liu, Hybrid nanoporous materials derived from ladder- and cage-type silsesquioxanes for water treatment, *ACS Appl. Nano Mater.* 3 (2) (2020) 1535–1541.
- [76] S. Ma, J. Xiong, R. Cui, X. Sun, L. Han, Y. Xu, Z. Kan, X. Gong, G. Huang, Effects of intermittent aeration on greenhouse gas emissions and bacterial community succession during large-scale membrane-covered aerobic composting, *J. Clean. Prod.* 266 (2020) 121551.
- [77] D.Y.C. Leung, G. Caramanna, M.M. Maroto-Valer, An overview of current status of carbon dioxide capture and storage technologies, *Renew. Sustain. Energy Rev.* 39 (2014) 426–443.
- [78] K. Pirzadeh, A.A. Ghoreyshi, S. Rohani, M. Rahimnejad, Strong influence of amine grafting on MIL-101 (Cr) metal-organic framework with exceptional CO₂/N₂ selectivity, *Ind. Eng. Chem. Res.* 59 (1) (2019) 366–378.
- [79] G. Chen, Y. Zhang, J. Xu, X. Liu, K. Liu, M. Tong, Z. Long, Imidazolium-based ionic porous hybrid polymers with POSS-derived silanols for efficient heterogeneous catalytic CO₂ conversion under mild conditions, *Chem. Eng. J.* 381 (2020) 122765.
- [80] J. Liang, A. Nuhnen, S. Millan, H. Breitzke, V. Gvilava, G. Buntkowsky, C. Janiak, Encapsulation of a porous organic cage into the pores of a metal-organic framework for enhanced CO₂ separation, *Angew. Chem., Int. Ed. Engl.* 59 (15) (2020) 6068–6073.
- [81] M.G. Mohamed, N.-Y. Liu, A.F.M. El-Mahdy, S.-W. Kuo, Ultrastable luminescent hybrid microporous polymers based on polyhedral oligomeric silsesquioxane for CO₂ uptake and metal ion sensing, *Microporous Mesoporous Mater.* 311 (2021) 110695.
- [82] S.-C. Qi, G.-X. Yu, D.-M. Xue, X. Liu, X.-Q. Liu, L.-B. Sun, Rigid supramolecular structures based on flexible covalent bonds: a fabrication mechanism of porous organic polymers and their CO₂ capture properties, *Chem. Eng. J.* 385 (2020) 123978.